Adaptive Voltage Control of Inverter-based DG in Active Distribution Networks with Measurement-Strategy Mapping Matrix

Ziqi Zhang, *Graduate Student Member, IEEE*, Peng Li, *Senior Member, IEEE*, Haoran Ji*, *Senior Member, IEEE*, Hao Yu, *Senior Member, IEEE*, Jinli Zhao, *Member, IEEE*, Wei Xi, Jianzhong Wu, *Fellow, IEEE*

***Abstract*—The high penetration of distributed generators (DGs) has exacerbated voltage violations in active distribution networks (ADNs). The sensitivity, as the law between nodal power injection and state variation, can be used to develop DG strategies efficiently. However, due to the nonlinearity, the accurate description and efficient application of ADN sensitivity have become an important challenge in the establishment of DG control strategy. In this paper, an adaptive voltage control strategy for DGs is developed based on ADN sensitivity. First, the measurement-strategy mapping matrix is established to describe the complex time-varying sensitivity. The sensitivity between nodal voltage and reactive power is described as discrete matrix elements, which are generated based on real-time measurements. Then, an adaptive voltage control model of DGs is built based on the measurement-strategy mapping matrix, in which the lifted linear decision rule (LLDR) is introduced to continue the discrete matrix elements as a couple of constraints. Efficient formulation of DG strategies is realized in a data-driven manner based on the ADN sensitivity. Finally, the effectiveness of the proposed strategy is validated using the modified IEEE 33-node system, practical 53-node system, and IEEE 123-node system. The proposed strategy can effectively cope with voltage problems while enhancing the adaptability to variations in practical operation.**

***Index Terms*—active distribution network (ADN), distributed generator (DG), voltage control, measurement-strategy mapping matrix.**

NOMENCLATURE

Set

Ω_{n}	Set of nodes in ADN
Ω_{b}	Set of branches in ADN
Ξ_i	Lifting decision space of node i

Indices

i, j, k	Indices of node, from 1 to N_{n}
ij	Indices of branch
s	Indices of expected reactive power variations, from 1 to N_{s}
t	Indices of time, from 1 to N_{t}
f	Indices of training object of the Koopman-based model, from 1 to N_{f}
n	Indices of the lift dimensions in the Koopman -based model, from 1 to N_{k}

Variable

$\varphi_{i,j,s}^{t}$	The sensitivity of voltage at node j to the sth reactive power variation at node i at period t
$\zeta_{ij,k,s}^{t}, \eta_{ij,k,s}^{t}$	The sensitivity of active/reactive power on branch ij to the sth reactive power variation at node k at period t
ΔQ_i^t	Variation of reactive power at node i at period t
$\Delta\hat{V}_{i,j}^{t+1}$	Estimated voltage variation at node j caused by power variations of node i at period $t+1$
$\Delta\hat{P}_{k,ij}^{t+1}$, $\Delta\hat{Q}_{k,ij}^{t+1}$	Estimated active/reactive power variation of branch ij caused by power variations of node k at period $t+1$
$\Delta\hat{V}_j^{t+1}$	Total estimated voltage variation of node j at period $t+1$
$\Delta\hat{P}_{ij}^{t+1}$, $\Delta\hat{Q}_{ij}^{t+1}$	Total estimated active/reactive power variation of branch ij at period $t+1$
$\hat{V}_j^t$	Estimated voltage at node j at period t
$\hat{P}_{ij}^{t}, \hat{Q}_{ij}^{t}$	Estimated active/reactive power of branch ij at period t
$\tilde{V}_j^t, \tilde{Q}_j^t$	The historical nodal voltage and nodal reactive power injection of ADN
$\xi_{i,s}^{t+1}$	The sth decision variable for the node i associated with the power deviation at period $t+1$
$\Delta Q_{i,s}$	The sth expected reactive power variations at node i
$P_{i,\mathrm{DG}}^{t+1}, Q_{i,\mathrm{DG}}^{t+1}$	Active/reactive power injection by DG at node i in period $t+1$

Parameter

N_{n}	Total number of nodes in ADN
N_{s}	Total number of expected power variations
N_{k}	Total number of lift dimensions in the Koopman operator
$N_{\mathrm{f}}, N_{\mathrm{l}}$	Total number of training/testing objects
N_{t}	Total periods of the time horizon
$V_{\mathrm{thr}}^{\max}, V_{\mathrm{thr}}^{\min}$	Upper/lower limit of the desired voltage range

This work was supported by the National Natural Science Foundation of China (U22B20114, 52307132) and Guizhou Provincial Science and Technology Projects under Grant [2023] General 292.

Z. Zhang, P. Li, H. Ji, J. Zhao, and H. Yu are with the Key Laboratory of Smart Grid of Ministry of Education, Tianjin University, Tianjin 300072, China (email: jihaoran@tju.edu.cn). (*Corresponding author: Haoran Ji*.)

W. Xi is with the Key Laboratory of Smart Grid of Ministry of Education, Tianjin University, Tianjin 300072, China, and also with the Novel Electric Power System (Beijing) Research Institute of China Southern Power Grid, Beijing 102209, China. (e-mail: xiwei@csg.cn).

J. Wu is with the Institute of Energy, School of Engineering, Cardiff University, Cardiff CF24 3AA, U.K. (email: wuj5@cardiff.ac.uk).

$V^{\min}, V^{\max}$ Upper/lower limit of the statutory voltage range
$S_{i,\mathrm{DG}}$ Capacity limit of DG at node i
$Q_i^{\max}, Q_i^{\min}$ Upper/lower limit of reactive power provided by DG at node i

Matrix

$\boldsymbol{\Phi}^t$ The voltage measurement-reactive power strategy mapping matrix at period t
$\boldsymbol{\Phi}_i^t$ The discrete sensitivity of the reactive power variation of node i to the voltage variation of each node at period t
$\boldsymbol{\Phi}_{i,j}^t$ The discrete sensitivity of the reactive power variation at node i on the voltage at node j at period t
$\boldsymbol{M}$ The weight matrix in the Koopman operator
$\boldsymbol{x}, \boldsymbol{y}$ Input/output of the Koopman operator
$\boldsymbol{x_l}$ Lifted dimension input of the Koopman operator
$\boldsymbol{X}, \boldsymbol{Y}$ The training set of the Koopman operator
$\boldsymbol{c}$ The base vector of the Koopman operator
$\boldsymbol{\delta}_{i,h}$ The hth extreme point of the lifting decision space of node i
$\boldsymbol{\xi}_i^{t+1}$ The decision vector for the node i associated with the power deviation at period $t+1$

I. Introduction

THE extensive integration of distributed generators (DGs) [1] gives rise to massive operational challenges in distribution networks [2]. Particularly, owing to the considerable inherent uncertainties [3], the high penetration of DGs [4] can potentially lead to severe voltage deviations in active distribution networks (ADNs) [5].

Various regulation devices have been implemented to enhance the voltage performance of ADNs [6]. Discrete regulation devices, such as on-load tap changers (OLTCs) and capacitor banks (CBs), predominantly function on longer timescales [7]. However, these devices encounter significant limitations due to their slow response times and limited action frequency [8], making them less effective in addressing frequent voltage fluctuations [9]. In contrast, the regulation of reactive power supply via DG inverter control offers a promising solution for achieving rapid voltage responses in ADNs [10]. DG inverters are typically designed with surplus capacity, which can be strategically utilized to regulate voltage levels within the ADN effectively [11].

Based on the network parameters of ADN, the physical-model-based method holds the promise of averting or mitigating overvoltage issues [12]. A reliability-constrained voltage control method was presented in [13] for DG inverters operating under uncertain conditions, which can reduce energy losses. In [14], a stochastic bilevel optimization model was proposed based on the ADN parameters to provide energy and grid services with DGs. In [15], a thermal battery equivalent model was established with precise ADN parameters to provide a voltage regulation service. The authors in [16] presented a multi-objective optimization model that could coordinate electric vehicle charging in ADN with DGs, aiming to address the interests of different stakeholders. A decentralized control strategy was presented in [17] that can significantly enhance the fairness in curtailing active power among inverters. A local voltage regulation method was proposed in [18], which utilized very short-term DG forecasts to circumvent imminent voltage violations. However, it may be difficult to obtain accurate ADN parameters in a complex operational environment, which limits the practical application of the physical-model-based method.

The data-driven-based method can realize the optimal operation of ADN based on the real-time measurement data or the historical data, without requiring an accurate mechanism model. A projection-embedded multi-agent deep reinforcement learning method was proposed in [19] to achieve a decentralized optimal for DGs to realize ADN voltage control. The authors in [20] proposed a data-driven-based distributed cooperative energy management system without an accurate mechanism model. A machine learning-assisted distributed algorithm was proposed in [21] to accelerate the solution of the Volt/Var control strategy.

As a quantitative representation of the control law of ADN, the sensitivity implies nodal connection relationship and line parameters, which can support a data-driven-based strategy formulation. The sensitivity of ADN has a clear physical concept that shows the relation of active or reactive power variation in voltage or current amplitude [23]. Considering the complex nonlinear characteristics of ADN, the precise sensitivity can be represented by a set of complex coupling high-dimensional equations to formulate DG control strategies effectively [24].

In terms of the acquisition methods, the sensitivity of ADN can be obtained through perturbation methods, model derivation, and data-driven approaches. The highest degree of accuracy in sensitivity acquisition can be achieved by applying power perturbations directly to the operational ADN system [25]. However, the implementation of the perturbation method may be constrained due to the potential disturbances introduced to the normal operation of the ADN. When the network parameters are accurately known, the sensitivity can be derived through the formulation of the physical model of the ADN [26]. Nonetheless, this approach may be limited by the precision of the available network parameters. With the increasing digitalization of distribution networks, a vast amount of real-time operational data has become accessible to distribution network operators [27]. This data abundance enables the extraction of crucial insights in a data-driven manner, including the analysis of system state variations [28]. By leveraging historical data of the ADN, it is possible to obtain sensitivity accurately, while avoiding the dependency on precise network parameters and the disturbances to the ADN operations.

In the application of ADN sensitivity, directly utilizing the high-dimensional nonlinear sensitivity poses significant challenges [29]. Through conducting a numerical linearization around the operating point, the linear sensitivity can be established for strategy formulation [30]. In [31], a local control function of photovoltaic (PV) inverters was established for real-time voltage regulation, in which the sensitivity of ADN is used as an alternative to power flow constraints. A robust data-driven sensitivity estimation approach was proposed in [32],

which has a high statistical efficiency to mitigate the impacts of unknown measurement noise. A fair nodal pricing method for distribution networks was proposed in [33], which can encourage demand-side users to participate in voltage regulation in ADN. Aiming at the coordination of multiple devices, a distributed voltage control strategy of ADNs was proposed in [34] with global sensitivities. However, due to the strong non-linear characteristics of the sensitivity, the utilization of linear regression may be inaccurate. Meanwhile, the voltage of ADN is deeply coupled with multi-node reactive power strategies, which makes the sensitivity-based strategy determination face difficulties, as shown in Fig. 1.

To realize a high-precision description and efficient application of ADN sensitivity, an adaptive voltage control strategy for DGs is proposed with the measurement-strategy mapping matrix. The main contributions are summarized as follows.

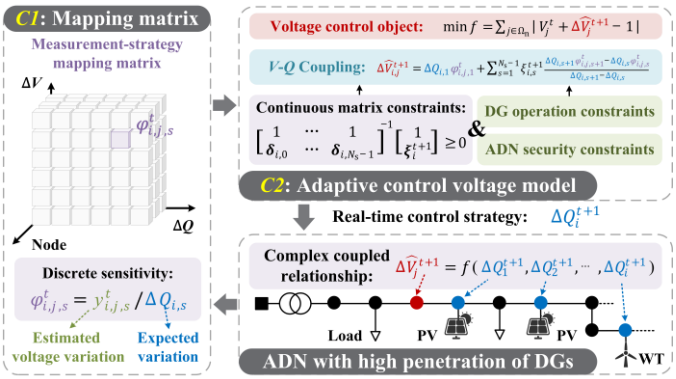

Fig. 1. The adaptive voltage control strategy for DGs

1) A voltage measurement-reactive power strategy mapping matrix of ADN is established to describe the complex time-varying sensitivity relationship, as shown in the left side of Fig. 1. Considering the significant nonlinearity of ADN sensitivity, the different dimensions of the mapping matrix are used to describe the effect of the power variations on different nodes and the magnitudes of power variations on the nodal voltage. The voltage-reactive power sensitivity of ADN can be described with the mapping matrix according to complex operation environment flexibly.

2) An adaptive voltage control model is established with the measurement-strategy mapping matrix, considering the coupling affected by the reactive power outputs from multiple DGs, as shown in the upper right part of Fig.1. To integrate the discrete mapping matrix into the voltage control model, the lifted linear decision rule (LLDR) is introduced to continue the matrix elements as a couple of constraints. Efficient real-time formulation of voltage control strategies for DGs can be achieved based on the sensitivity of ADN.

The remainder of this paper is organized as follows. In Section II, the measurement-strategy mapping matrix is established according to the real-time voltage measurement of ADN. In Section III, an adaptive voltage control model for DGs is built with the continuous measurement-strategy mapping matrix. The case studies using the modified IEEE 33-node distribution system, 53-node practical distribution system, and IEEE 123-node distribution system are presented in Section IV. Finally, conclusions are stated in Section V.

II. Data-driven Measurement-strategy Mapping Matrix Generation

The voltage-reactive power sensitivity of ADN serves as a quantitative depiction of the impact of nodal reactive power variations on nodal voltage. In this section, a mapping matrix is established to realize an accurate description of the sensitivity between nodal voltage and nodal reactive power injection.

A. Measurement-strategy mapping matrix

The sensitivity exhibits high dimensional and nonlinear characteristics, which cannot be accurately described by a single linear function. In this paper, a three-dimensional measurement-strategy mapping matrix $\boldsymbol{\Phi}^t_{[N_\mathrm{n}]\times[N_\mathrm{n}]\times[N_\mathrm{s}]}$ is established to describe the sensitivity between nodal power variations and voltage variations, as shown in (1).

$$\boldsymbol{\Phi}_i^t=\begin{bmatrix}\boldsymbol{\Phi}_{i,1}^t\\ \boldsymbol{\Phi}_{i,2}^t\\ \vdots\\ \boldsymbol{\Phi}_{i,j}^t\\ \vdots\\ \boldsymbol{\Phi}_{i,N_\mathrm{n}}^t\end{bmatrix}=\begin{bmatrix}\varphi_{i,1,1}^t & \cdots & \varphi_{i,1,s}^t & \cdots & \varphi_{i,1,N_\mathrm{s}}^t\\ \varphi_{i,2,1}^t & \cdots & \varphi_{i,2,s}^t & \cdots & \varphi_{i,2,N_\mathrm{s}}^t\\ \vdots & & \vdots & & \vdots\\ \varphi_{i,j,1}^t & \cdots & \varphi_{i,j,s}^t & \cdots & \varphi_{i,j,N_\mathrm{s}}^t\\ \vdots & & \vdots & & \vdots\\ \varphi_{i,N_\mathrm{n},1}^t & \cdots & \varphi_{i,N_\mathrm{n},s}^t & \cdots & \varphi_{i,N_\mathrm{n},N_\mathrm{s}}^t\end{bmatrix}\quad \forall i\in\{1,2,\cdots,N_\mathrm{n}\} \tag{1}$$

where $\boldsymbol{\Phi}_i^t$ represents the sensitivity of the reactive power variation of node i to the voltage variation of each node at period t. $\varphi_{i,j,s}^t$ denotes the sensitivity of node j with a reactive power variation $\Delta Q_{i,s}$ at node i in period t, which can be described as follows.

$$\varphi_{i,j,s}^t=\lim_{\Delta Q_{i,s}\to 0}\Delta V_j^t/\Delta Q_{i,s}\,,s=1,\ldots,N_\mathrm{s} \tag{2}$$

By selecting different power variations $\Delta Q_{i,s}$ as the sampling points, the voltage measurement-reactive power strategy mapping matrix describes the nonlinear sensitivity relationship on a point-by-point basis. The high dimensional characteristics of voltage-power sensitivity can be described more accurately.

***Remark 1*:** The sensitivity between active power and nodal voltage can also be constructed as the matrix form in (1). Considering the demand for renewable energy consumption, the active power of DGs is assumed cannot be reduced in this paper. The influence of the variations of active power strategy is not discussed in the following discussion.

Remark 2: The variation in the nodal reactive power strategy will also cause the variations in the line's active/reactive power in addition to nodal voltage. Considering the effect of the reactive power variations at different nodes on the line power, the line measurement-reactive power strategy mapping matrix can be described as Eq. (3):

$$\boldsymbol{\Phi}_i^{t,\rho}=\begin{bmatrix}\boldsymbol{\Phi}_{i,1}^{t,\rho}\\ \boldsymbol{\Phi}_{i,2}^{t,\rho}\\ \vdots\\ \boldsymbol{\Phi}_{i,l}^{t,\rho}\\ \vdots\\ \boldsymbol{\Phi}_{i,N_l}^{t,\rho}\end{bmatrix}=\begin{bmatrix}\varphi_{i,1,1}^{t,\rho} & \cdots & \varphi_{i,1,s}^{t,\rho} & \cdots & \varphi_{i,1,N_\mathrm{s}}^{t,\rho}\\ \varphi_{i,2,1}^{t,\rho} & \cdots & \varphi_{i,2,s}^{t,\rho} & \cdots & \varphi_{i,2,N_\mathrm{s}}^{t,\rho}\\ \vdots & & \vdots & & \vdots\\ \varphi_{i,l,1}^{t,\rho} & \cdots & \varphi_{i,l,s}^{t,\rho} & \cdots & \varphi_{i,l,N_\mathrm{s}}^{t,\rho}\\ \vdots & & \vdots & & \vdots\\ \varphi_{i,N_l,1}^{t,\rho} & \cdots & \varphi_{i,N_l,s}^{t,\rho} & \cdots & \varphi_{i,N_l,N_\mathrm{s}}^{t,\rho}\end{bmatrix}\quad \forall i\in\{1,2,\cdots,N_\mathrm{n}\},\rho\in\{\mathrm{PL},\mathrm{QL}\} \tag{3}$$

where $\varphi_{i,l,s}^{t,\rho}$ represents the sensitivity of reactive power injection at node i on the active/reactive power variations at line l.

The sensitivity between branch current and nodal reactive power injection can also be constructed as the matrix form in (1). Since the branch current can be expressed as (4), only three ADN sensitivities of voltage, branch active power, and reactive power are necessary to determine DG control strategies.

$$I_{ij}^{t} = \sqrt{\left(P_{ij}^{t}\right)^2 + \left(Q_{ij}^{t}\right)^2}/V_i^t \tag{4}$$

In the following analysis, only the voltage-reactive power sensitivity is examined. Other sensitivities can be obtained and applied using similar methods which will not be elaborated upon.

***Remark 3*:** The establishment of the measurement-strategy mapping matrix only needs the data of the critical nodes in ADN. In terms of voltage measurements, the voltage of the critical nodes is required, such as the measurement of the grid-connected nodes of DGs, the nodes with key loads, and some nodes with two more branches. In terms of the reactive power strategy, only the strategy of the node with controllable resources is necessary.

B. Koopman-based mapping matrix generation

Considering the complex operation environment, the accurate generation of the voltage measurement-reactive power strategy mapping matrix is realized based on the Koopman operator in this sub-section.

The Koopman operator, as an effective data analysis tool, can extract the hidden logic in the data of ADN. In this paper, the Koopman operator is trained to extract the voltage-reactive power sensitivity of various scenarios day ahead and construct the mapping matrix during the intra-day operation based on the real-time measurements.

Koopman operator is proposed for a discrete and nonlinear dynamical system described by (5), aiming to form an evolution on a smooth manifold [35].

$$\boldsymbol{y} = f(\boldsymbol{x}) \tag{5}$$

The Koopman operator is defined as a linear operator $\boldsymbol{K}$, which can map the nonlinear function $f(\cdot)$ to a new function $(\boldsymbol{K}w)(\cdot)$, as shown in (6).

$$\begin{aligned} (\boldsymbol{K}f)(\boldsymbol{x}) &= f\big(g(\boldsymbol{x})\big) \\ \boldsymbol{K}\rho_d(\boldsymbol{x}) &= \mu_d \cdot \rho_d(\boldsymbol{x}), d = 1,2,\cdots,\infty \end{aligned} \tag{6}$$

where the $\rho_d(\cdot)$ and μ_d are the Koopman eigenfunctions and eigenvalues respectively. $f(\cdot)$ is defined as the scalar-valued observable functions.

Assuming that N_d dimensional expansion terms are considered, the nonlinear relationship between $\boldsymbol{x}$ and $\boldsymbol{y}$ can be expressed as a linear form approximately, which is shown as follows.

$$\boldsymbol{y} \approx \sum_{d=1}^{N_\mathrm{d}} m_d\, \rho_d(\boldsymbol{x}) \tag{7}$$

According to (7), there is a weight coefficients matrix $\boldsymbol{M}$ that satisfies the linear mapping relationship approximately, in which $\rho(\cdot)$ is replaced by $\boldsymbol{x}_l$ as shown in (8).

$$\boldsymbol{y} = \boldsymbol{M}\boldsymbol{x}_l = \boldsymbol{M}\begin{bmatrix}\boldsymbol{x}\\ \boldsymbol{\chi}(\boldsymbol{x})\end{bmatrix} \tag{8}$$

where $\boldsymbol{\chi}(\boldsymbol{x})$ is the approximation to the Koopman eigenfunctions, which is represented by the lift-dimension function of the input vector. When N_k dimensions are required to be lifted in the practical operation, the basic mathematical structure of $\boldsymbol{\chi}(\boldsymbol{x})$ can be described as (9).

$$\begin{aligned} \boldsymbol{\chi}(\boldsymbol{x}) &= \begin{bmatrix}\chi_1(\boldsymbol{x}) & \cdots & \chi_n(\boldsymbol{x}) & \cdots & \chi_{N_\mathrm{k}}(\boldsymbol{x})\end{bmatrix}^\mathrm{T} \\ \chi_k(\boldsymbol{x}) &= \sqrt{\textstyle\sum_{m=1}^{N_\mathrm{m}}(x_k - c_{km})^2}\cdot\log\sqrt{\textstyle\sum_{m=1}^{N_\mathrm{m}}(x_k - c_{km})^2} \\ &\forall k \in \{1,2,\ldots,N_\mathrm{k}\} \end{aligned} \tag{9}$$

where $\boldsymbol{c_k} \in \mathbb{R}_{N_\mathrm{m}\times 1}$ is the base vector of the kth lifted dimension, which can be chosen randomly from the interval of the variable range. N_m denotes the dimension of $\boldsymbol{x}$, as well as the total number of the input feature.

To portray the nonlinear sensitivity, nodal voltage at period t and nodal reactive power variation at period $t+1$ are taken as the inputs $\boldsymbol{x}$, while the voltage variation of each node at period $t+1$ is taken as the outputs $\boldsymbol{y}$.

In the day-ahead stage, a training set is built based on the historical operational data of ADN, as shown in (10). Each training object includes the input vector and the output vector.

$$\begin{aligned} &\begin{cases}\boldsymbol{X} = \begin{bmatrix}\boldsymbol{x}^{(1)} & \boldsymbol{x}^{(2)} & \cdots & \boldsymbol{x}^{(N_\mathrm{f})}\end{bmatrix} \\ \boldsymbol{Y} = \begin{bmatrix}\boldsymbol{y}^{(1)} & \boldsymbol{y}^{(2)} & \cdots & \boldsymbol{y}^{(N_\mathrm{f})}\end{bmatrix}\end{cases} \\ \boldsymbol{x} &= \begin{bmatrix}\tilde{V}_1^t & \cdots & \tilde{V}_{N_\mathrm{n}}^t & \Delta\tilde{Q}_1^{t+1} & \cdots & \Delta\tilde{Q}_{N_\mathrm{n}}^{t+1}\end{bmatrix}^\mathrm{T} \\ \boldsymbol{y} &= \begin{bmatrix}\Delta\tilde{V}_1^{t+1} & \cdots & \Delta\tilde{V}_j^{t+1} & \cdots & \Delta\tilde{V}_{N_\mathrm{n}}^{t+1}\end{bmatrix}^\mathrm{T} \\ \Delta\tilde{V}_j^{t+1} &= \tilde{V}_j^{t+1} - \tilde{V}_j^t, \forall j \in \{1,\cdots,N_\mathrm{n}\} \\ \Delta\tilde{Q}_j^{t+1} &= \tilde{Q}_j^{t+1} - \tilde{Q}_j^t, \forall j \in \{1,\cdots,N_\mathrm{n}\} \end{aligned} \tag{10}$$

where $\tilde{V}_j^t$ and $\tilde{Q}_j^t$ denote the historical data of ADN.

Based on the historical data, the weight coefficients matrix $\boldsymbol{M}$ in (8) can be determined by the least square estimation method day ahead, storing the potential laws between voltage measurement and reactive power variations. The least-square estimation can be described as (11).

$$\begin{aligned} \boldsymbol{M} &= \boldsymbol{Y}\boldsymbol{X}_\mathbf{L}^\mathrm{T}\left[\boldsymbol{X}_\mathbf{L}\boldsymbol{X}_\mathbf{L}^\mathrm{T}\right]^\dagger \\ \boldsymbol{X}_\mathbf{L} &= \begin{bmatrix}\boldsymbol{x}^{(1)} & \cdots & \boldsymbol{x}^{(f)} & \cdots & \boldsymbol{x}^{(N_\mathrm{f})} \\ \boldsymbol{\chi}(\boldsymbol{x}^{(1)}) & \cdots & \boldsymbol{\chi}(\boldsymbol{x}^{(f)}) & \cdots & \boldsymbol{\chi}(\boldsymbol{x}^{(N_\mathrm{f})})\end{bmatrix} \end{aligned} \tag{11}$$

where $[\cdot]^\dagger$ denotes Moore-Penrose inverse matrix operation.

During the intra-day operation, the trained Koopman operator is used to update the measurement-strategy mapping matrix based on real-time measurements.

First, the ADN voltage measurements $\boldsymbol{V}^t$ of critical nodes and the expected reactive power variations $\Delta\widehat{\boldsymbol{Q}}_i^{t+1}$ of the nodes with controllable resources are formed as an input vector $\boldsymbol{x}_{i,s}^t$, which can be described as (12).

$$\begin{aligned} \boldsymbol{x}_{i,s}^t &= \begin{bmatrix}\boldsymbol{V}^t & \Delta\widehat{\boldsymbol{Q}}_i^{t+1}\end{bmatrix}^\mathrm{T}, \forall i \in \{1,\cdots,N_\mathrm{n}\} \\ \boldsymbol{V}^t &= \begin{bmatrix}V_1^t & \cdots & V_{N_\mathrm{n}}^t\end{bmatrix}^\mathrm{T} \\ \Delta\widehat{\boldsymbol{Q}}_i^{t+1} &= [0 \quad \cdots \quad \Delta Q_{i,s} \quad \cdots \quad 0]^\mathrm{T}, \forall i \in \{1,\cdots,N_\mathrm{n}\} \end{aligned} \tag{12}$$

Then, the elements $\varphi_{i,j,s}^t$ in the voltage measurement -reactive power strategy mapping matrix can be obtained based on the trained Koopman operator, as shown in (13).

$$\varphi_{i,j,s}^{t} = y_{i,j,s}^{t}/\Delta Q_{i,s}$$

$$[y_{i,1,s}^{t} \quad \cdots \quad y_{i,j,s}^{t} \quad \cdots \quad y_{i,N_n,s}^{t}]^{\mathrm{T}} = \boldsymbol{M}\begin{bmatrix} \boldsymbol{x}_{i,s}^{t} \\ \boldsymbol{\chi}(\boldsymbol{x}_{i,s}^{t}) \end{bmatrix} \tag{13}$$

$$\forall i,j \in \{1,\cdots,N_n\}, \forall s \in \{1,\cdots,N_s\}$$

It is worth noting that the data quality of historical data affects the accuracy of the Koopman operator, which in turn affects the accurate estimation of the measure-strategy mapping matrix. The adverse effect of bad data and measurement errors in historical data can be eliminated by data preprocessing. The processed data can support the accurate portrayal of complex sensitivity relationships.

In the practical operation of ADN, the advanced metering infrastructure (AMI) [36] may obtain a 15-minute average value of the measurement. In this case, the average value can be used as training data to train the Koopman operator. With the integration of the supervisory control and data acquisition (SCADA) [37] and the distribution-level phasor measurement unit (D-PMU) [38], minute-level or even second-level synchronized measurements can be utilized to train the Koopman operator.

In summary, the voltage measurement-reactive power strategy mapping matrix can be generated in a data-driven manner during intra-day operation. Relying on the real-time voltage measurement and expected power variations, a high-precision description of nonlinear sensitivity will be realized under a complex ADN environment.

III. Adaptive Voltage Control with Continuous Measurement-Strategy Mapping Matrix

In the practical operation of ADN, the nodal voltage variation is coupling affected by the multiple DG reactive power outputs, forming a complex optimization problem. In this section, an adaptive voltage control model is established based on the measurement-strategy mapping matrix. Efficient control strategy formulation can be achieved with the application of ADN sensitivity.

A. LLDR-based continuation of the measurement-strategy mapping matrix

The measurement-strategy mapping matrix gives an accurate description of the complex sensitivity between nodes. However, due to the elements in the matrix are discrete, it is difficult to be integrated into the adaptive voltage control model. Moreover, nodal voltage variation is affected by the coupling of reactive power output from multiple DGs, which makes it difficult to determine the respective optimal strategy of each DG based on a single sensitivity. Thus, the lifted linear decision rule is applied in this section to realize the continuation of the discrete measurement-strategy mapping matrix. A couple of continuous constraints will be obtained, in which the matrix elements are used as the segmentation points.

Taking the voltage-reactive power sensitivity between nodes i and j as an example, the segmented linearized sensitivity can be described as follows.

$$\Delta Q_i^{t+1} = \alpha_{i,j,s}\Delta Q_{i,s} + \alpha_{i,j,s+1}\Delta Q_{i,s+1}, \text{if } \Delta Q_i^{t+1} \in [\Delta Q_{i,s}, \Delta Q_{i,s+1}] \tag{14}$$

$$\Delta \hat{V}_{i,j}^{t+1} = \alpha_{i,j,s}\varphi_{i,j,s}^{t}\Delta Q_{i,s} + \alpha_{i,j,s+1}\varphi_{i,j,s+1}^{t}\Delta Q_{i,s+1}$$

$$\alpha_{i,j,s} + \alpha_{i,j,s+1} = 1, \forall i,j \in \{1,\cdots,N_n\}, s \in \{1,\cdots,N_s\}$$

where, $\alpha_{i,j,s}$ is the auxiliary variable.

Due to the non-linear threshold in (14), an auxiliary variable $\xi_{i,s}^{t+1}$ is introduced to describe the specific location of current power variation in the range $[\Delta Q_{i,s}, \Delta Q_{i,s+1}]$. The value of auxiliary variables can be expressed by the following mathematical formula.

$$\xi_{i,s}^{t+1} = \begin{cases} \min\{\Delta Q_i^{t+1}, \Delta Q_{i,s+1}\}, s = 1 \\ \max\{\min\{\Delta Q_i^{t+1}, \Delta Q_{i,s+1}\} - \Delta Q_{i,s}, 0\}, s = 2, \ldots, N_s - 2 \\ \max\{\Delta Q_i^{t+1} - \Delta Q_{i,s}, 0\}, s = N_s - 1 \end{cases} \tag{15}$$

The value of $\xi_{i,s}^{t+1}$ within different ranges is shown in Fig. 2, where the horizontal axis indicates the values of the original variable and the vertical axis indicates the values of the auxiliary variable. The auxiliary variable $\xi_{i,s}^{t+1}$ takes linearly increasing in the range $[\Delta Q_{i,s}, \Delta Q_{i,s+1}]$ and takes a constant value as 0 or the length of the range $\Delta Q_{i,s+1} - \Delta Q_{i,s}$ outside.

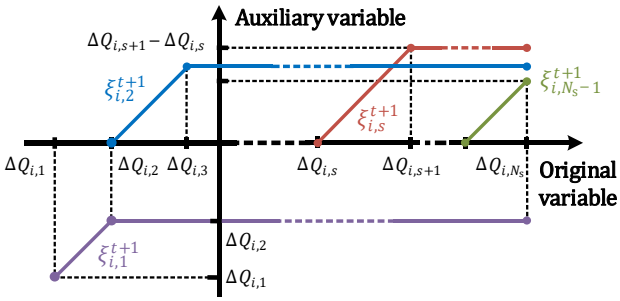

Fig. 2. The auxiliary variable for node i

Therefore, the nodal power variation can be expressed as follows.

$$\Delta Q_i^{t+1} = \sum_{s=1}^{N_s-1} \xi_{i,s}^{t+1} \tag{16}$$

Let $\boldsymbol{\xi}_i^{t+1}$ denote the vector for node i of the auxiliary variable $[\xi_{i,1}^{t+1}, \ldots, \xi_{i,N_s-1}^{t+1}]^{\mathrm{T}}$, whose feasible domain Ξ_i is non-convex. $\boldsymbol{\xi}_i^{t+1}$ can be uniquely determined by the extreme point of Ξ_i, as shown in (17).

$$\begin{cases} \boldsymbol{\xi}_i^{t+1} = \sum_{h=0}^{N_s-1} \lambda_{i,h}^{t+1}\boldsymbol{\delta}_{i,h} \\ \sum_{h=0}^{N_s-1} \lambda_{i,h}^{t+1} = 1, \lambda_{i,0}^{t+1}, \lambda_{i,1}^{t+1}, \ldots, \lambda_{i,N_s-1}^{t+1} \geq 0 \end{cases} \tag{17}$$

where, $\boldsymbol{\delta}_{i,h}$ denotes the hth extreme point of Ξ_i, which can be calculated by the expected reactive power variations $\Delta Q_{i,s}$ in the measurement-strategy mapping matrix. The extreme point of Ξ_i is defined as (18).

$$\begin{cases} \boldsymbol{\delta}_{i,0} = [\Delta Q_{i,1}, 0, \ldots, 0]^{\mathrm{T}} \\ \boldsymbol{\delta}_{i,1} = [\Delta Q_{i,2}, 0, \ldots, 0]^{\mathrm{T}} \\ \boldsymbol{\delta}_{i,2} = [\Delta Q_{i,2}, \Delta Q_{i,3} - \Delta Q_{i,2}, \ldots, 0]^{\mathrm{T}} \\ \vdots \\ \boldsymbol{\delta}_{i,N_s-1} = [\Delta Q_{i,2}, \ldots, \Delta Q_{i,N_s} - \Delta Q_{i,N_s-1}]^{\mathrm{T}} \end{cases} \tag{18}$$

To simplify the expression, Eq. (17) can be further expressed in matrix form as shown in (19).

$$\begin{bmatrix} 1 & \ldots & 1 \\ \boldsymbol{\delta}_{i,0} & \ldots & \boldsymbol{\delta}_{i,N_s-1} \end{bmatrix} [\lambda_{i,0}^{t+1} \quad \ldots \quad \lambda_{i,N_s-1}^{t+1}]^{\mathrm{T}} = \begin{bmatrix} 1 \\ \boldsymbol{\xi}_i^{t+1} \end{bmatrix} \tag{19}$$

$$\lambda_{i,0}^{t+1}, \lambda_{i,1}^{t+1}, \dots, \lambda_{i,N_s-1}^{t+1} \geq 0$$

Since $\lambda_{i,h}^{t+1}$ is non-negative, the Eq. (19) can be transformed into the following constraints, that is the continuous mapping matrix constraints for the nodal voltage to the reactive power.

$$\begin{bmatrix} 1 & \dots & 1 \\ \boldsymbol{\delta}_{i,0} & \dots & \boldsymbol{\delta}_{i,N_s-1} \end{bmatrix}^{-1} \begin{bmatrix} 1 \\ \boldsymbol{\xi}_i^{t+1} \end{bmatrix} \geq 0 \tag{20}$$

In summary, based on the lifted linear decision rule, the discrete elements of the measurement-strategy mapping matrix are expressed as a couple of continuous constraints. The voltage-reactive power sensitivity constrained between two segment points is determined by linear interpolation. The continuous measurement-strategy mapping matrix will be used to establish the voltage control model of ADN.

B. Adaptive voltage control model with continuous mapping matrix

To efficiently determine the control strategies for DGs, an adaptive voltage control model is constructed with the continuous measurement-strategy mapping matrix.

The voltage deviations over the technical limits jeopardize the electricity supply. Especially, the extreme situation of voltage deviation may lead to the load cutting of ADN. Thus, the object function is selected to minimize the extent of voltage deviation from the desired range $\left[V_{\text{thr}}^{\min}, V_{\text{thr}}^{\max}\right]$, as formulated in Eq. (21).

$$\min f_{\text{V}} = \sum_{j\in\Omega_{\text{n}}} \left|\hat{V}_j^{t+1} - 1\right|, \hat{V}_j^{t+1} \geq V_{\text{thr}}^{\max} || \hat{V}_j^{t+1} \leq V_{\text{thr}}^{\min} \tag{21}$$

where $\hat{V}_j^{t+1}$ is the estimation of the voltage variation on node j.

Considering the nodal voltage variation is coupling affected by DG outputs on multiple nodes, the estimated voltage variation of node j can be further described as follows:

$$\Delta\hat{V}_j^{t+1} = \sum_{i=1}^{N_{\text{n}}} \Delta\hat{V}_{i,j}^{t+1}, \forall j \in \{1,2,\cdots,N_{\text{n}}\} \tag{22}$$

where the voltage variation $\Delta\hat{V}_{i,j}^{t+1}$ at node j caused by the reactive power variation ΔQ_i^{t+1} at node i can be calculated as the following equation.

$$\begin{gathered} \Delta\hat{V}_{i,j}^{t+1} = \Delta Q_{i,1}\varphi_{i,j,1}^{t} + \sum_{s=1}^{N_s-1} \xi_{i,s}^{t+1} \frac{\Delta Q_{i,s+1}\varphi_{i,j,s+1}^{t} - \Delta Q_{i,s}\varphi_{i,j,s}^{t}}{\Delta Q_{i,s+1} - \Delta Q_{i,s}} \\ \forall i,j \in \{1,2,\cdots,N_{\text{n}}\} \end{gathered} \tag{23}$$

Meanwhile, to ensure the security operation of ADN, the security constraints should be further integrated into the adaptive voltage control model, as shown as follows.

$$\begin{gathered} V^{\min} \leq \hat{V}_j^{t+1} \leq V^{\max} \\ \hat{V}_j^{t+1} = V_j^{t} + \Delta\hat{V}_j^{t+1} \end{gathered} \tag{24}$$

where V_j^t is the real-time voltage measurement.

Given the limitations of DG operation, the operation constraints of DG also need to be integrated into the adaptive voltage control model, which is shown as follows.

$$\begin{gathered} Q_i^{\min} \leq Q_{i,\text{DG}}^{t+1} \leq Q_i^{\max} \\ Q_{i,\text{DG}}^{t+1} \leq \sqrt{\left(S_{i,\text{DG}}\right)^2 - \left(P_{i,\text{DG}}^{t+1}\right)^2} \\ Q_{i,\text{DG}}^{t+1} = Q_{i,\text{DG}}^{t} + \Delta Q_i^{t+1}, \forall i \in \left\{1,2,\cdots,N_{\text{g}}\right\} \end{gathered} \tag{25}$$

Based on the above analysis, the adaptive voltage control model can be expressed in the following form.

$$\begin{gathered} \min f_{\text{V}} = \sum_{j\in\Omega_{\text{n}}} \left|\hat{V}_j^{t+1} - 1\right|, \hat{V}_j^{t+1} \geq V_{\text{thr}}^{\max} || \hat{V}_j^{t+1} \leq V_{\text{thr}}^{\min} \\ \text{s.t.} \quad (16), (18), (20), (22), (23), (24), (25) \end{gathered} \tag{26}$$

As for the nonlinear threshold function in (21), the auxiliary variable ϑ_j^{t+1} is introduced to express the extent of voltage deviation and some equivalent constraints are added as follows.

$$\begin{gathered} \min f_{\text{V}} = \sum_{j\in\Omega_{\text{n}}} \vartheta_j^{t+1} \\ \vartheta_j^{t+1} \geq \hat{V}_j^{t+1} - V_{\text{thr}}^{\max} \\ \vartheta_j^{t+1} \leq -\hat{V}_j^{t+1} + V_{\text{thr}}^{\min} \\ \vartheta_j^{t+1} \geq 0 \end{gathered} \tag{27}$$

Thus, after the linearization relaxation, the original model is converted into a linear programming (LP) model, as shown in (28), which can be solved by commercial solvers, such as GUROBI and CPLEX.

$$\begin{gathered} \min f_{\text{V}} = \sum_{j\in\Omega_{\text{n}}} \vartheta_j^{t+1} \\ \text{s.t.} \quad (16), (18), (20), (22), (23), (24), (25), (27) \end{gathered} \tag{28}$$

***Remark 4*:** The other control objectives can also be taken into account in the adaptive control model. As an example, the economic operation object can be introduced to minimize the total active power losses, as shown in (29).

$$\min f_{\text{L}} = \sum_{ij\in\Omega_{\text{b}}} r_{ij} I_{ij,t}^2 \tag{29}$$

However, accurate ADN parameters may be not available in the practical operation. Meanwhile, the voltage $V_{i,t}$ is typically around 1.0 p.u. in normal operation. Thus, Eq. (29) can be approximately converted to Eq. (30).

$$\min f_{\text{L}} = \sum_{ij\in\Omega_{\text{b}}} \left(\left(\hat{P}_{ij}^{t+1}\right)^2 + \left(\hat{Q}_{ij}^{t+1}\right)^2\right) \tag{30}$$

At the same time, the constraints related to the active and reactive power of the branch should be further appended, as shown in (31).

$$\begin{gathered} \Delta\hat{P}_{k,ij}^{t+1} = \Delta Q_{k,1}\zeta_{ij,k,1}^{t} + \sum_{s=1}^{N_s-1} \xi_{k,s}^{t+1} \frac{\Delta Q_{k,s+1}\zeta_{ij,k,s+1}^{t} - \Delta Q_{k,s}\zeta_{ij,k,s}^{t}}{\Delta Q_{k,s+1} - \Delta Q_{k,s}} \\ \forall k \in \Omega_{\text{n}}, \forall ij \in \Omega_{\text{b}} \\ \Delta\hat{Q}_{k,ij}^{t+1} = \Delta Q_{k,1}\eta_{ij,k,1}^{t} + \sum_{s=1}^{N_s-1} \xi_{k,s}^{t+1} \frac{\Delta Q_{k,s+1}\eta_{ij,k,s+1}^{t} - \Delta Q_{k,s}\eta_{ij,k,s}^{t}}{\Delta Q_{k,s+1} - \Delta Q_{k,s}} \\ \forall k \in \Omega_{\text{n}}, \forall ij \in \Omega_{\text{b}} \\ \Delta\hat{P}_{ij}^{t+1} = \sum_{k=1}^{N_{\text{n}}} \Delta\hat{P}_{k,ij}^{t+1}, \forall ij \in \Omega_{\text{b}} \\ \Delta\hat{Q}_{ij}^{t+1} = \sum_{k=1}^{N_{\text{n}}} \Delta\hat{Q}_{k,ij}^{t+1}, \forall ij \in \Omega_{\text{b}} \\ \hat{P}_{ij}^{t+1} = P_{ij}^{t} + \Delta\hat{P}_{ij}^{t+1} \\ \hat{Q}_{ij}^{t+1} = Q_{ij}^{t} + \Delta\hat{Q}_{ij}^{t+1} \end{gathered} \tag{31}$$

Thus, an adaptive voltage control model is established based on the continuous measurement-strategy mapping matrix. By flexibly adjusting the reactive power of multiple DGs, voltage fluctuations in ADN can be effectively suppressed in a complex operation environment.

The proposed method is essentially a centralized data-driven-based control method, which can also be extended to a decentralized framework. By forming a local model based on the mapping matrix in each ADN area, the decentralized

framework can reduce the computation burden effectively.

C. Implementation of the adaptive voltage control strategy

The practical implementation of the proposed method can be divided into the day-ahead stage and the intra-day operation stage, as shown in Fig. 3.

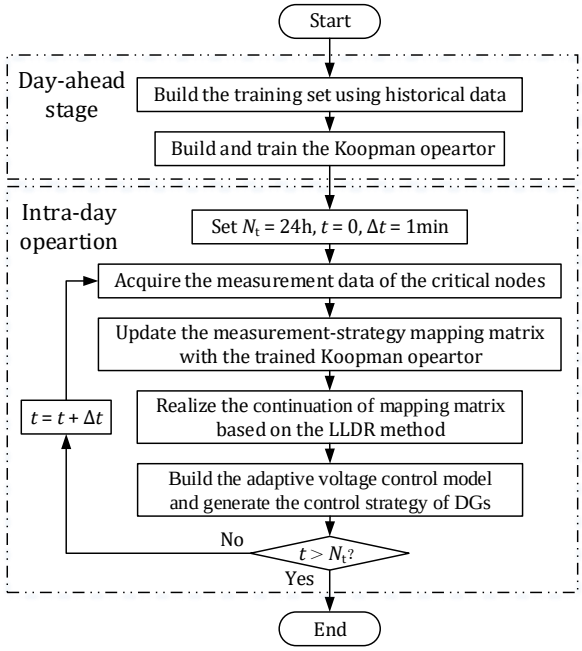

Fig. 3. Schematic of the proposed adaptive voltage control strategy

1) In the day-ahead stage, a Koopman operator is built in the distribution management system (DMS) of ADN, which is trained by the historical operational data. The trained Koopman operator can realize an accurate generation of the nonlinear sensitivity of ADN.

2) During the intra-day operation, the measurement-strategy mapping matrix of ADN is first generated based on the real-time measurement of the critical nodes. For the continuous connection of discrete matrix elements, the lifted linear decision rule is utilized to construct the linear measurement-strategy mapping constraints. Then, an adaptive voltage control model is established in each control interval, which can determine the control strategies for DGs. By regulating the reactive outputs of DGs in real-time operation, the proposed method can address the voltage violations of ADN effectively.

***Note that*:** the control interval in the proposed method is flexible, which only needs to be longer than the strategy formulation time. Typically, strategies can be generated in seconds based on the proposed method. Thus, the control window and measurement sampling rate can be minimized to a few seconds.

***Remark 5*:** Communication is required in the proposed method, while communication delays will affect the measurement uploading and the strategy release. However, the delay of communication generally does not exceed 1 second [39], while the control strategy of DGs in the proposed method is updated every 1 minute. Thus, the affection of communication delay is relatively limited in the practical application of the proposed method.

IV. Case Studies and Analysis

In this section, the effectiveness of the proposed adaptive voltage control strategy for DGs is verified using the modified IEEE 33-node distribution system, 53-node practical distribution system, and IEEE 123-node distribution system. The numerical experiments were conducted on a computer with an Intel(R) Core(TM) i7-9750H CPU processor running at 2.60 GHz and 16 GB of RAM.

A. Modified IEEE 33-node system

The modified IEEE 33-node distribution system includes a substation and 32 branches, of which the rated voltage level is 12.66 kV. The structure of the test system is shown in Fig. 4.

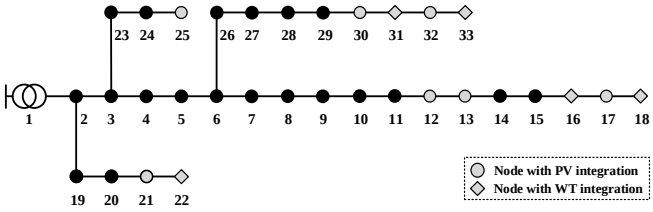

Fig. 4. Structure of the modified IEEE 33-node system

The total active power and reactive power demands of ADN are 3715 kW and 2300 kvar. To consider the impact of DGs, 7 PV units with 200 kVA capacity each and 5 WT units with 300 kVA capacity are integrated into the test system. The real-time fluctuation curves of DG generation, including PVs and WTs, and load operation are shown in Fig. 5 to Fig. 7. The upper and lower limits of the statutory voltage range are set as 1.10 p.u. and 0.90 p.u.

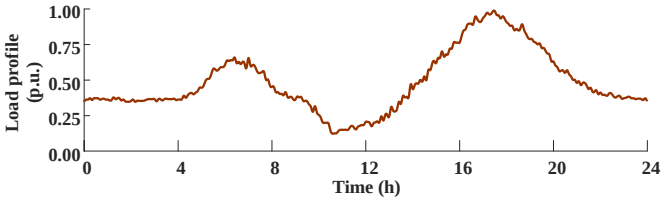

Fig. 5. The fluctuation curves of the load

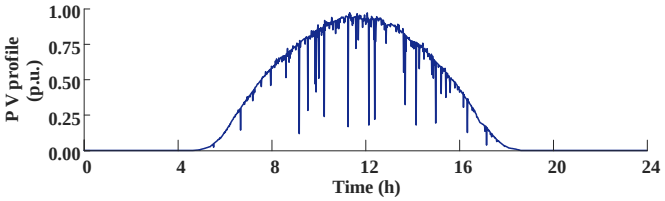

Fig. 6. The fluctuation curves of PV

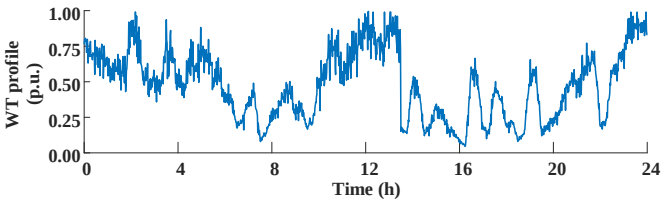

Fig. 7. The fluctuation curves of WT

1) Accuracy analysis of the generated mapping matrix

To realize an accurate description of the nonlinear sensitivity, the measurement-strategy mapping matrix is generated based

on the Koopman operator. Taking the voltage-reactive power sensitivity of ADN as an example, nonlinear complex sensitivity be described based on the mapping matrix in a segmented linearized manner.

From the perspective of the relationship at a single node, the mapping matrix can accurately depict the nonlinear sensitivity between nodal voltage and the nodal reactive power. The effects of different scenarios are illustrated in Fig. 8. Compared to the linear relationship derived at the operating point, the estimated mapping matrix demonstrates higher accuracy in describing this complex relationship. Additionally, when compared to the most accurate sensitivity obtained through the perturbation method, the proposed method offers similar accuracy in a segmented linearized manner while avoiding disturbances to the ADN.

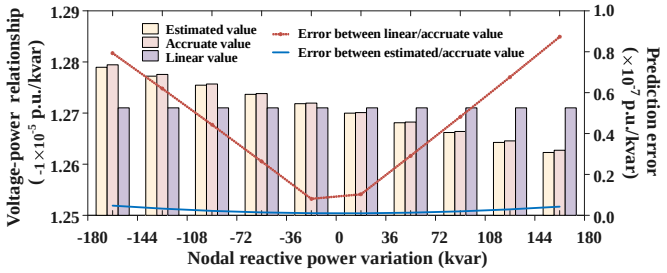

Fig. 8. The comparison of the accuracy between different scenarios

Regarding adaptability to complex ADN environments, the Koopman operator demonstrates robust generalization capabilities. The distribution of the prediction error, depicted in Fig. 9, shows that the estimation error between the predicted and actual values remains predominantly below 1%. This high level of accuracy can adapt to the varying states of ADN.

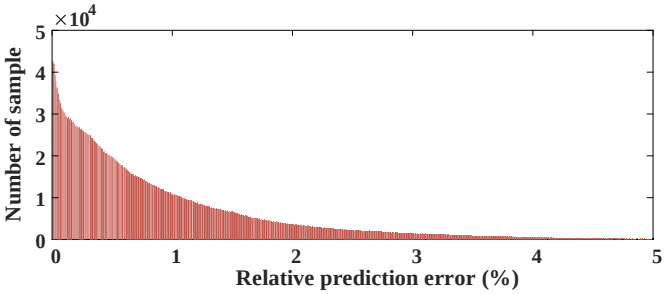

Fig. 9. The distribution of the prediction error

To quantitatively evaluate the performance of the trained Koopman operator, the mean absolute error (MAE) is used as the numerical evaluation index, defined as Eq. (32):

$$\mathrm{MAE} = \frac{1}{N_\mathrm{l} \times N_\mathrm{n}} \sum_{n=1}^{N_\mathrm{l}} \sum_{i=1}^{N_\mathrm{n}} \left| \hat{y}_{n,i} - y_{n,i} \right| \tag{32}$$

where $\hat{y}_{n,i}$ and $y_{n,i}$ are the predicted value and the true value of the sensitivity, respectively. N_l is the total number of test objects. N_n is the total number of nodes in ADN.

The MAE index represents the average absolute value of the prediction error, which is 8.20×10^{-6} on the test set, demonstrating that the predicted sensitivity is very close to the real value. Consequently, an accurate depiction of the sensitivity mapping relationship between voltage measurements and reactive power strategy is achievable within the complex operational environment of the ADN.

2) Effectiveness analysis of voltage control strategy

To verify the effectiveness and advancement of the proposed adaptive voltage control strategy, the voltage control object f_V is first taken as an example to be analyzed, and five scenarios are adopted in this paper.

Scenario I: There is no control strategy conducted on DG units, where the initial operational state of the ADN can be obtained.

Scenario II: The strategies of DGs are determined based on the continuous measurement-strategy mapping matrix of the voltage and reactive power with the proposed voltage control method.

Scenario III: The control strategies of DGs are determined based on the linear sensitivity relationship obtained at the operating point based on existing methods.

Scenario IV: The real-time centralized model-based method is used to optimize the DG strategy, which can achieve a theoretically optimal control effect for the ADN.

Scenario V: The iterative data-driven method in [40] is used to determine the DG control strategy.

The voltage deviation index (VDI) is involved to intuitively reflect the optimization effect of the proposed method, which can be described by Eq. (33).

$$\mathrm{VDI} = \sum_{t=1}^{N_\mathrm{t}} \sum_{j \in \Omega_\mathrm{n}} \left| \left(V_j^t\right)^2 - 1 \right| \tag{33}$$

The optimization results for the five scenarios are listed in Table I.

TABLE I
OPTIMIZATION RESULTS OF THE FIVE SCENARIOS

Scenario	Maximum voltage (p.u.)	Minimum voltage (p.u.)	VDI (p.u.)
I	1.0588	0.9227	1449.58
II	1.0151	0.9695	276.37
III	1.0151	0.9695	284.15
IV	1.0162	0.9695	269.32
V	1.0153	0.9695	321.95

The comparison of Scenarios I and II is used to validate the effectiveness of the proposed method. In Scenario I, the high-penetration DG units lead to frequent voltage fluctuation and voltage deviation. The voltage distribution of the system in Scenario I is shown in Fig. 10.

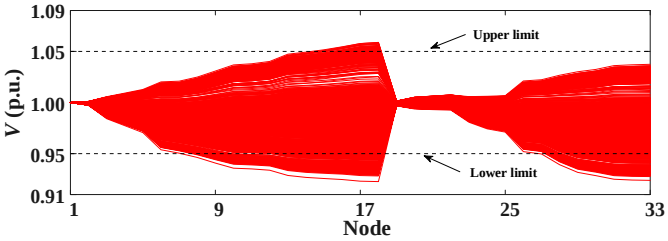

Fig. 10. Voltage profiles in Scenario I

Fig. 11 shows the voltage distribution of the system in Scenario II. Using the continuous voltage measurement-reactive power strategy mapping matrix, the adaptive voltage control model is built during the intra-day operation. By updating reactive power control strategies in real-time according to ADN measurements, the voltage control strategies can be determined

adaptively. Taking the DG at node 17 as an example, the reactive power is flexibly adjusted according to the fluctuation in the complex operational environment of ADN, as shown in Fig. 12. Compared with the initial operation state in Scenario I, the voltage deviation of ADN is significantly alleviated.

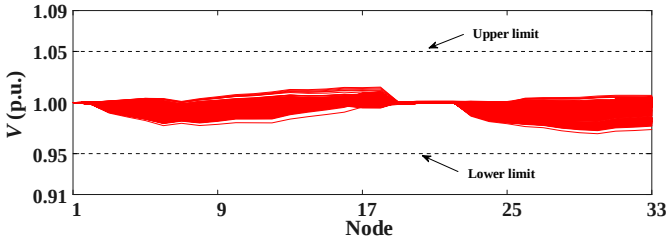

Fig. 11. Voltage profiles in Scenario II

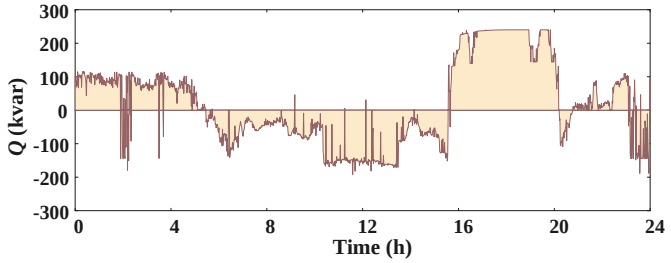

Fig. 12. Reactive power of DGs at node 17 in Scenario II

It is worth noting that accurate sensitivity can be obtained based on the perturbation method. However, due to the coupling of nodal voltages of ADN with the output of multiple DGs, accurate sensitivity cannot be directly used to obtain control strategies for DGs. Therefore, some studies have proposed to realize the superposition calculation by inscribing the sensitivity relationship among nodes in a linear form, as in Scenario III. Due to the linear relationship ignores the non-linear characteristics of the inter-node effects, Scenario III is less effective in voltage optimization, as shown in Fig. 13. In contrast, an accurate portrayal of ADN sensitivity is realized based on the continuous mapping matrix in Scenario II, which can support a more effective formulation of DG strategies. The impact on the mapping accuracy of sensitivity can be obtained by comparing the control effect of Scenarios II and III.

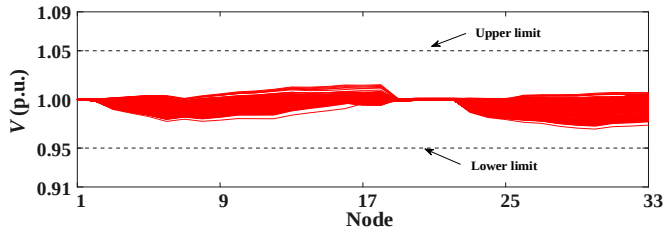

Fig. 13. Voltage profiles in Scenario III

The comparison of Scenarios II and IV is used to verify the indistinctive gap between the proposed method and the theoretical optimization result. Fig. 14 shows the voltage distribution of the system in Scenario IV. The centralized model-based method constructs a global optimization model with accurate network parameters of ADN. Through making real-time decisions on the control strategy of DGs, a global optimal voltage control effect can be obtained. However, this may not be available in reality due to the communication constraints. Thus, the real-time centralized model-based method can only yield a theoretically optimal control effect. In comparison, the proposed method in Scenario II obtains a similar control effect based on the concealed logic between nodes of ADN. The formulation of the control strategy for DGs is achieved with the sensitivity of ADN in a data-driven manner.

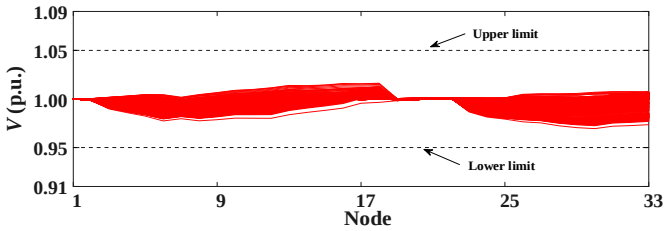

Fig. 14. Voltage profiles in Scenario IV

The comparison of Scenarios II and V is used to demonstrate the advantages of the proposed method. The data-driven method in Scenario V can respond to system state changes based on the measurement data, which can improve the operational performance in complex environments. The voltage distribution of the system in Scenario V is shown in Fig. 15.

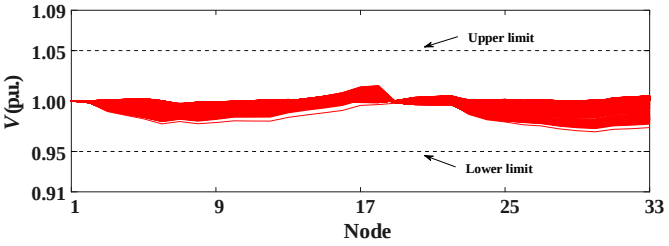

Fig. 15. Voltage profiles in Scenario V

However, the interactive iteration is used to realize an operation control of DGs. Taking the strategy determination process at 19: 00, the data-driven method in Scenario V uses 29 iterations to converge at a stable solution, as shown in Fig. 16, which may cause sustained perturbations on ADN during the control process. Compared with iterative data-driven methods, the proposed method does not require an iterative process, which can achieve real-time strategy optimization, avoiding the impact on ADN's normal operation effectively.

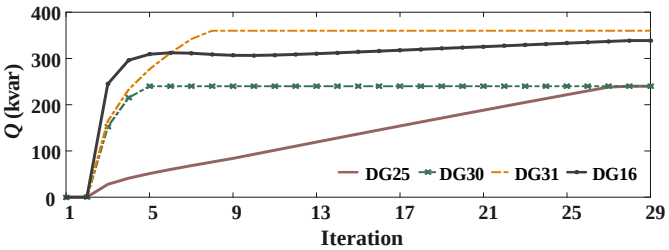

Fig. 16. Iterations of DG strategy in Scenario V

3) Adaptability to multiple control objectives

The economic operation object can also be considered in the proposed method with the sensitivity of ADN. In this sub-section, a numerical analysis is presented for minimizing both voltage deviation and network losses. The objective function can be formulated as follows.

$$\min f = \omega_1 f_{\mathrm{L}} + \omega_2 f_{\mathrm{V}} \tag{34}$$

where, ω_1 and ω_2 are the weight coefficients associated with power loss and voltage deviation.

The network loss of ADN is used to analysis the control performance, which can be calculated as shown in Eq. (35).

$$\mathrm{PLoss} = \sum_{t=1}^{N_{\mathrm{t}}} \sum_{ij \in \Omega_{\mathrm{b}}} \left(I_{ij}^{t}\right)^2 r_{ij} \tag{35}$$

where, r_{ij} is the resistance of branch ij.

The scenario settings are the same as those in Section IV.A.2). The optimization results under the combined control object for the five scenarios are listed in Table II.

TABLE II
OPTIMIZATION RESULTS OF THE FIVE SCENARIOS

Scenario	Maximum voltage (p.u.)	Minimum voltage (p.u.)	VDI (p.u.)	PLoss (kWh)	Total loss (VDI+PL)
I	1.0588	0.9227	1449.58	1002.61	2452.19
II	1.0465	0.9645	604.77	758.80	1363.58
III	1.0556	0.9575	785.28	641.42	1426.71
IV	1.0452	0.9625	614.54	747.61	1362.15
V	1.0148	0.9694	329.67	1318.00	1647.67

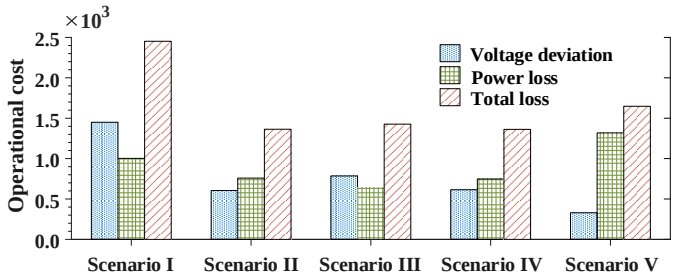

Fig. 17. The comparison of operational cost under five scenarios

Fig. 17 shows the comparison of operational costs under five scenarios. Because of the lack of control, the network loss in Scenario I is large. In contrast, Scenario II uses the measurement-strategy mapping matrix to accurately depict the sensitivity of ADN. The flexible adjustment of the DG control strategy is realized, effectively reducing the network loss while obtaining a similar effect to the theoretical optimal control method in Scenario IV. In Scenario III, the linear approximation ignores the high dimensional error of the sensitivity, resulting in a decrease in the control effect. In contrast, better voltage control effects are realized in Scenario III, but not as effective in reducing network losses.

4) Influence of the segments in measurement-strategy matrix

The number of linear segments, that is the number of expected reactive power changes $\Delta Q_{i,s}$, is an important parameter in the measurement-strategy mapping matrix. The increasing number of segments will increase the size of the optimization model, resulting in a slower solution speed. To quantitatively analyze the effect of the number of segment points, different N_{s} values are set in this paper to compare the optimal control effect and the solving time of Scenario II. The optimization results are shown in Table III.

The visual representation of the segments' influence is shown in Fig. 18. The increase in the number of segment points results in an increase in the number of variables introduced for the continuation of the measurement-strategy mapping matrix. This will increase the computational burden prominently. Therefore, the solution time of the adaptive voltage control model becomes gradually longer.

TABLE III
INFLUENCE OF THE NUMBER OF LINEAR SEGMENTS

Value	Maximum voltage (p.u.)	Minimum voltage (p.u.)	VDI (p.u.)	Solution time (s)
$N_{\mathrm{s}} = 11$	1.0151	0.9695	276.37	3.01
$N_{\mathrm{s}} = 21$	1.0151	0.9695	276.38	6.36
$N_{\mathrm{s}} = 31$	1.0151	0.9695	276.37	14.18
$N_{\mathrm{s}} = 41$	1.0151	0.9695	276.41	22.51
$N_{\mathrm{s}} = 51$	1.0151	0.9695	276.36	31.04

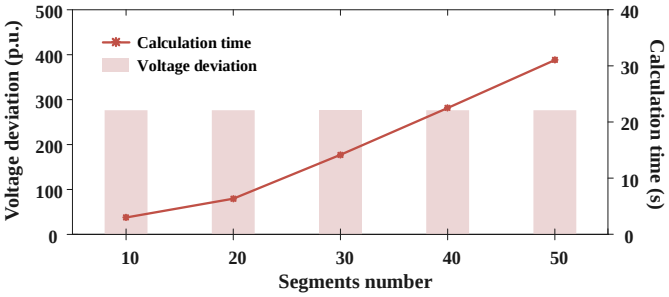

Fig. 18. The influence of the segments in the measurement-strategy matrix

5) Influence of the key measurements on measurement-strategy mapping matrix

When ADN is partially monitored, the measurement mapping matrix can be constructed based on the measurements from the critical node. The control effect and computation time under the partially monitored scenario are analyzed in this sub-section, as shown in Table IV. In the test system, nodes 2, 3, 6, 12, 13, 16, 17, 18, 21, 22, 25, 30, 31, 32, and 33 are set as the critical node equipped with measurements, while the other nodes have no measurement devices.

TABLE IV
COMPARISON OF CONTROL EFFECT UNDER KEY MEASUREMENTS

Scenario	Maximum voltage (p.u.)	Minimum voltage (p.u.)	VDI (p.u.)	Solution time (s)
II. Fully monitored	1.0151	0.9695	276.3708	3.01
II. Partially monitored	1.0151	0.9695	299.0251	1.97

It can be seen from the data that there is a significant decrease in the computation time when only key measurements are utilized in the establishment of the mapping matrix, while the control effect remains almost the same.

B. Practical application

To further illustrate the adaptability in practical power grids of the proposed adaptive voltage control strategy for DGs, a test case from a practical system in Guangzhou of China is further adopted. The structure of the system is shown in Fig. 19.

The system consists of 52 lines, with a rated voltage level of 10 kV, and the total active power and reactive power demands are 8790 kW and 1786 kvar, respectively. To simulate the impact on ADN caused by high penetration of DGs, 19 PV units and 5 WT units are integrated into the test system. The locations and capacities of DGs are shown in Table V. The

penetration rate of DG reaches almost 120%. The scenario settings are similar to those in Section IV.A, which are not illustrated here.

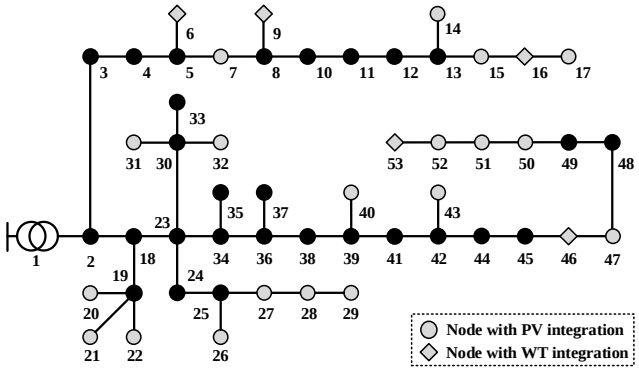

Fig. 19. Structure of HXF23 53-node practical distribution system

The optimization results for the five scenarios are listed in Table VI. Similar to the conclusions in Section IV-A, the proposed proposed adaptive voltage control strategy can effectively mitigate voltage violations. The voltage profiles of the whole system in Scenarios I, II, III, IV, and V, are shown in Fig. 20 to Fig. 24.

TABLE V
BASIC INSTALLATION PARAMETERS OF DGS

Location	Type	Capacity (kVA)
6, 9, 16, 46, 53	WT	300
7, 14, 15, 17, 40, 43,47, 50, 51, 52	PV	200
20, 21, 22, 26, 27,28, 29, 31, 32	PV	360

TABLE VI
OPTIMIZATION RESULTS OF THE FIVE SCENARIOS

Scenario	Maximum voltage (p.u.)	Minimum voltage (p.u.)	VDI (p.u.)
I	1.0562	0.9201	2466.27
II	1.0248	0.9760	207.50
III	1.0248	0.9589	930.19
IV	1.0248	0.9760	191.05
V	1.0145	0.9760	275.36

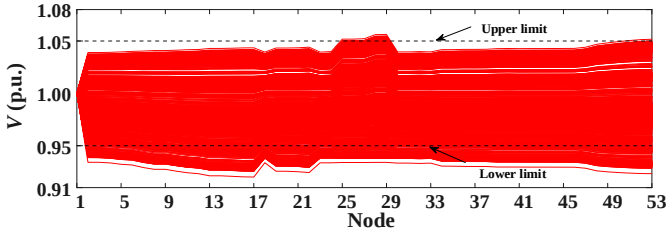

Fig. 20. Voltage profiles in Scenario I

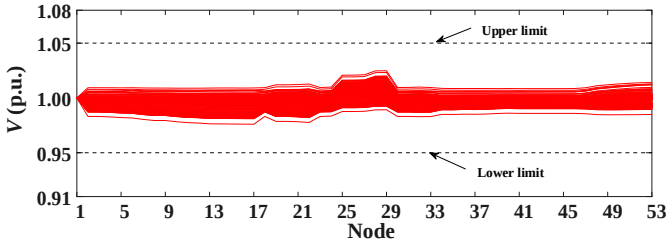

Fig. 21. Voltage profiles in Scenario II

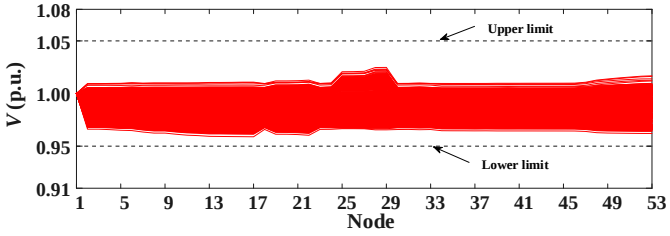

Fig. 22. Voltage profiles in Scenario III

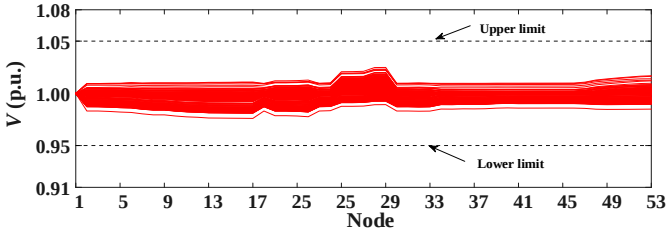

Fig. 23. Voltage profiles in Scenario IV

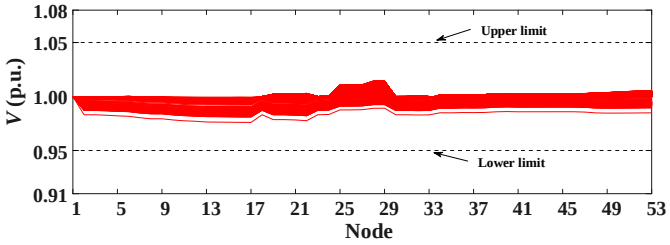

Fig. 24. Voltage profiles in Scenario V

C. Scalability validation

The modified IEEE 123-node system is adopted to verify the scalability of the proposed method on a large-scale ADN, as shown in Fig. 25. The rated voltage level is 4.16 kV. The total active and reactive power loads on the system are 3490 kW and 1920 kvar.

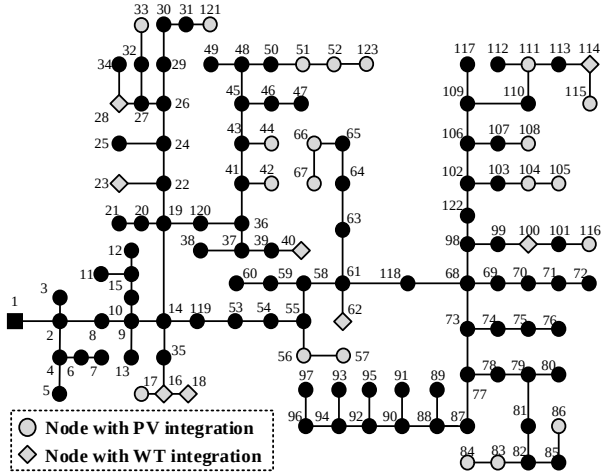

Fig. 25. Structure of the modified IEEE 123-node system

To simulate the impact of high penetration of DGs, 21 PV units with 400 kVA capacity each and 8 WT units with 600 kVA capacity are integrated into the test system. The scenario settings are the same as those in Section IV.A. The optimization results for the five scenarios are listed in Table VII. The voltage profiles of the whole system in Scenarios I, II, III, IV, and V, are shown in Fig. 26 to Fig. 30.

TABLE VII
OPTIMIZATION RESULTS OF THE FIVE SCENARIOS

Scenario	Maximum voltage (p.u.)	Minimum voltage (p.u.)	VDI (p.u.)
I	1.0970	0.9004	8993.48
II	1.0082	0.9893	544.77
III	1.0066	0.9858	1298.20
IV	1.0082	0.9891	492.61
V	1.0149	0.9943	594.82

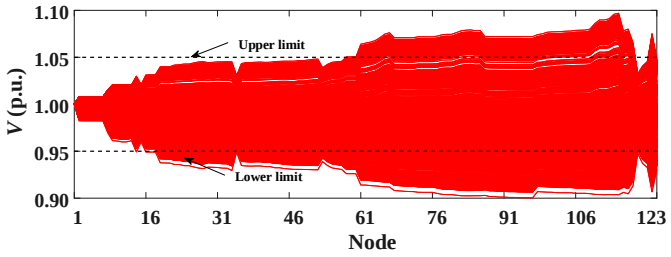

Fig. 26. Voltage profiles in Scenario I

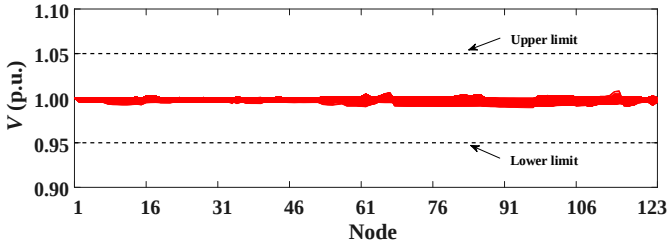

Fig. 27. Voltage profiles in Scenario II

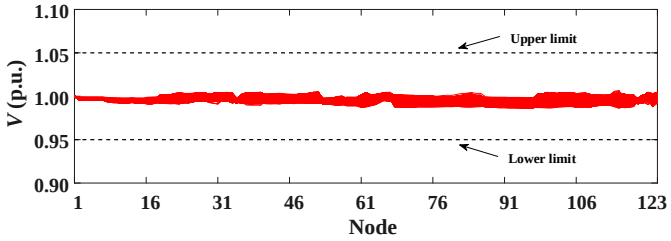

Fig. 28. Voltage profiles in Scenario III

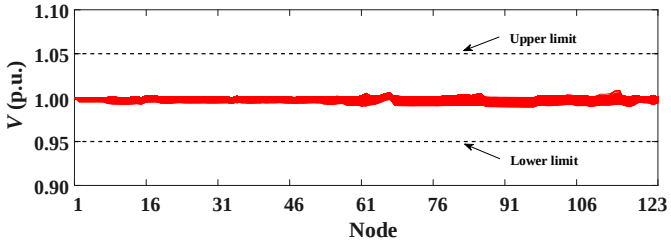

Fig. 29. Voltage profiles in Scenario IV

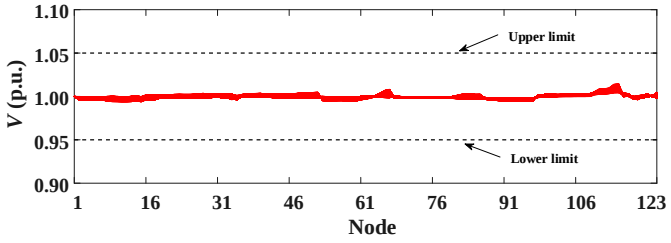

Fig. 30. Voltage profiles in Scenario V

Similarly, by the coordination of multiple DGs, the voltage fluctuations can be effectively mitigated based on the proposed method, which takes about 15 seconds for the solution of the adaptive voltage control model. As can be seen in Table VII, the proposed method has a similar voltage control performance compared with the theoretically optimal effect in Scenario IV. Meanwhile, compared with the linear sensitivity-based control method in Scenario III, the proposed method can greatly improve the control effect by improving the accuracy of sensitivity description. Compared to Scenario V, the proposed method can provide better control performance avoiding perturbing the normal operation of ADN.

To analyze the relationship between the computation complexity and the size of ADN, the proposed IEEE 33-node system, HXF23 53-node system, and IEEE 123-node system are taken as examples. The numerical result is shown in Table VIII. It can be seen from the data that the computational complexity rises as the system size increases. Meanwhile, the computation time shows an approximate linear growth trend with the number of nodes in ADN. However, the calculations can all be done in seconds in the above systems.

TABLE VIII
COMPUTATION TIME UNDER DIFFERENT ADN SIZES

Test system	Number of nodes	Computation time (s)
IEEE33	33	3.01
HXF23	53	7.58
IEEE123	123	15.24

In summary, the proposed strategy can realize an efficient operation of ADN based on the high-precision sensitivity. A flexible control strategy can be determined according to the complex operation environment adaptively.

V. CONCLUSIONS

To effectively mitigate voltage violations in the complex environment, a sensitivity-based voltage control strategy for DGs is proposed with a measurement-strategy mapping matrix. First, the Koopman operator is trained to generate the measurement-strategy mapping matrix. The test results show that the Koopman operator can extract the hidden logic in the data of ADN effectively. Meanwhile, the complex time-varying relationship between nodal voltage and the power strategy can be characterized accurately by the three-dimensional mapping matrix. Then, the mapping matrix is continued based on the lifted linear decision rule, which can be integrated into the optimization model. As shown in the numerical analysis, an efficient formulation of DG control strategies can be realized considering multi-node voltage to reactive power coupling. Compared with the linear sensitivity-based method, the control effect of the proposed method is better, which is similar to that of the centralized method. Enhanced control performance can be achieved through the adaptive application of sensitivity.

Several notable issues warrant further research. In consideration of the impact of communication, how to ensure effectiveness in the case of communication failure is one of the problems that needs to be solved. In addition, considering the different scenarios in the practical operational environment, the event handler-based mechanism may need to be further introduced to adaptively select the objective function.

REFERENCES

[1] S. Li, Z. Li, X. Wan, *et al*, "Recent progress in flexible organic solar cells," *eScience*, vol. 3, no. 1, 100085, 2023.

[2] J. Jian, J. Zhao, H. Ji, *et al*, "Supply restoration of data centers in flexible distribution networks with spatial-temporal regulation," *IEEE Trans. Smart Grid*, vol. 15, no. 1, pp. 340-354, 2024.

[3] A. Tavakoli, S. Saha, M. Arif, *et al*. "Impacts of grid integration of solar PV and electric vehicle on grid stability, power quality and energy economics: a review," *IET Energy Syst. Int.*, vol. 2, no. 3, pp. 243-260, 2020.

[4] H. S. Salama, G. Magdy, A. Bakeer, *et al*. "Adaptive coordination control strategy of renewable energy sources, hydrogen production unit, and fuel cell for frequency regulation of a hybrid distributed power system," *Prot. Control Mod. Power Syst.*, vol. 7, 34, 2022.

[5] J. Zhang, T. Wang, J. Chen, *et al.* "Cluster voltage control method for "whole county" distributed photovoltaics based on improved differential evolution algorithm," *Front. Energy*, vol. 17, pp.782-795, 2023.

[6] X. Chen, M. Mcelroy, Q. Wu, *et al*. "Transition towards higher penetration of renewables: an overview of interlinked technical, environmental and socio-economic challenges," *J. Mod. Power Syst. Clean Energy*, vol.7, no. 1, pp.1-8, 2019.

[7] T. Tewari, A. Mohapatra, S. Anand. "Coordinated control of OLTC and energy storage for voltage regulation in distribution network with high PV penetration," *IEEE Trans. Sustain. Energy*, vol. 12, no. 1, pp. 262-272, 2021.

[8] Y. Gao, N. Yu. "Model-augmented safe reinforcement learning for Volt-VAR control in power distribution networks," *Appl. Energy*, vol. 313, 118762, 2022.

[9] Z. Zhang, F. Silva, Y. Guo, *et al*. "Double-layer stochastic model predictive voltage control in active distribution networks with high penetration of renewables," *Appl. Energy*, vol. 302, 117530, 2021.

[10] J. Xiao, G. Zu, H. Zhou, *et al*. "Total quadrant security region for active distribution network with high penetration of distributed generation," *J. Mod. Power Syst. Clean Energy*, vol. 9, no. 1, pp. 128-137, 2021.

[11] Y. Guo, Q. Wu, H. Gao, *et al*. "MPC-based coordinated voltage regulation for distribution networks with distributed generation and energy storage system," *IEEE Trans. Sustain. Energy*, vol. 10, no. 4, pp. 1731-1739, 2019.

[12] Z. Zhang, P. Li, H. Ji, *et al.* "Combined central-local voltage control of inverter-based DG in active distribution networks," *Appl. Energy*, vol. 372, 123813, 2024.

[13] Q. Chai, C. Zhang, Y. Xu, *et al*. "PV inverter reliability-constrained Volt/Var control of distribution networks," *IEEE Trans. Sustain. Energy*, vol. 12, no. 3, pp. 1788-1800, 2021.

[14] A. Ravi, L. Bai, V. Cecchi, *et al.* "Stochastic strategic participation of active distribution networks with high-penetration DERs in wholesale electricity markets," *IEEE Trans. Smart Grid*, vol. 14, no. 2, pp. 1515-1527, 2023.

[15] Y. Hua, Q. Xie, H. Hui, *et al.* "Use of inverter-based air conditioners to provide voltage regulation services in unbalanced distribution networks," *IEEE Trans. Power Deliv.*, vol. 38, no. 3, pp. 1569-1579, 2023.

[16] Y. Wang, H. Wang, R. Razzaghi, *et al.* "Multi-objective coordinated EV charging strategy in distribution networks using an improved augmented epsilon-constrained method," *Appl. Energy*, vol. 369, 123547, 2024.

[17] Y. Gerdroodbari, R. Razzaghi, F. Shahnia. "Decentralized control strategy to improve fairness in active power curtailment of PV inverters in low-voltage distribution networks," *IEEE Trans. Sustain. Energy*, vol. 12, no. 4, pp. 2282-2292, 2021.

[18] S. Ghosh, S. Rahman, M. Pipattanasomporn. "Distribution voltage regulation through active power curtailment with PV inverters and solar generation forecasts," *IEEE Trans. Sustain. Energy*, vol. 8, no. 1, pp. 13-22, 2017.

[19] M. Zhang, G. Guo, S. Magnusson, *et al.* "Data driven decentralized control of inverter based renewable energy sources using safe guaranteed multi-agent deep reinforcement learning," *IEEE Trans. Sustain. Energy*, vol. 15, no. 2, pp. 1288-1299, 2024.

[20] J. Li, Q. Zhou, Y. He, *et al.* "Distributed cooperative energy management system of connected hybrid electric vehicles with personalized non-stationary inference," *IEEE Trans. Transp. Electrif.*, vol. 8, no. 2, pp. 2996-3007, 2022.

[21] B. Li, Q. Xu. "A machine learning-assisted distributed optimization method for inverter-based Volt-VAR control in active distribution networks," *IEEE Trans. Power Syst.*, vol. 39, no. 2, pp. 2668-2681, 2024.

[22] A. Malekpour, A. Annaswamy, J. Shah. "Hierarchical hybrid architecture for volt/var control of power distribution grids," *IEEE Trans. Power Syst.*, vol. 35, no. 2, pp. 854-863, 2020.

[23] S. Talkington, D. Turizo, S. Grijalva, *et al*. "Conditions for estimation of sensitivities of voltage magnitudes to complex power injections," *IEEE Trans. Power Syst.*, vol. 39, no. 1, pp. 478-491, 2024.

[24] J. Dancker, M. Wolter, "Power-transfer-distribution-factor-based sensitivity factors for integrated energy systems," *IEEE Trans. Sustain. Energy*, vol. 15, no. 1, pp. 486-498, 2024.

[25] K. Ye, J. Zhao, F. Ding, et al. "Global sensitivity analysis of large distribution system with PVs using deep gaussian process," *IEEE Trans. Power Syst.*, vol. 36, no. 5, pp. 4888-4891, 2021.

[26] S. Maharjan, A. M. Khambadkone, J. C.-H. Peng, "Robust Constrained Model Predictive Voltage Control in Active Distribution Networks," *IEEE Trans. Sustain. Energy*, vol. 12, no. 1, pp. 400-411, 2021.

[27] T. Xu, W. Wu, Y. Hong, *et al*, "Data-driven inverter-based Volt/VAr control for partially observable distribution networks," *CSEE J. Power Energy Syst.*, vol. 9, no. 2, pp. 548-560, 2023.

[28] J. Zhao, Z. Zhang, H. Yu, *et al*. "Cloud-edge collaboration based local voltage control for DGs with privacy preservation," *IEEE Trans. Ind. Inform.*, vol. 19, no. 1, pp. 98-108, 2023.

[29] C. Flynn, A. B. Pengwah, R. Razzaghi, *et al*. "An improved algorithm for topology identification of distribution networks using smart meter data and its application for fault detection," *IEEE Trans. Smart Grid*, vol. 14, no. 5, pp. 3850-3861, 2023.

[30] Z. Zhang, C. Dou, D. Yue, *et al*. "Voltage sensitivity-related hybrid coordinated power control for voltage regulation in ADNs," *IEEE Trans. Smart Grid*, vol. 15, no. 2, pp. 1388-1398, 2024.

[31] Y. Gao, X. Xu, Z. Yan, *et al*. "Robust parametric programming for adaptive piecewise linear control of photovoltaic inverters to regulate voltages in power distribution systems," *IEEE Trans. Power Syst.*, vol. 39, no. 2, pp. 3685-3700, 2024.

[32] Y. Liang, J. Zhao, P. Siano, *et al*. "Temporally-adaptive robust data-driven sparse voltage sensitivity estimation for large-scale realistic distribution systems with PVs," *IEEE Trans. Power Syst.*, vol. 38, no. 4, pp. 3977-3980, 2023.

[33] B. Li, C. Wan, P. Yu, *et al*. "Voltage-price coupling in distribution networks," *IEEE Trans. Smart Grid*, vol. 15, no. 2, pp. 1438-1449, 2024.

[34] P. Yu, C. Wan, M. Sun, *et al*. "Distributed voltage control of active distribution networks with global sensitivity," *IEEE Trans. Power Syst.*, vol. 37, no. 6, pp. 4214-4228, 2022.

[35] L. Guo, Y. Zhang, X. Li, *et al*. "Data-driven power flow calculation method: a lifting dimension linear regression approach," *IEEE Trans. Power Syst.*, vol. 37, no. 3, pp. 1798-1808, 2022.

[36] Q. Sun, H. Li, Z. Ma, *et al.* "A comprehensive review of smart energy meters in intelligent energy networks," *IEEE Internet Things J.*, vol. 3, no. 4, pp. 464-479, 2016.

[37] S. Huang, C. Lu, Y. Lo. "Evaluation of AMI and SCADA data synergy for distribution feeder modeling," *IEEE Trans. Smart Grid*, vol. 6, no. 4, pp. 1639-1647, 2015.

[38] J. Yang, H. Yu, P. Li, *et al.* "Real-time D-PMU data compression for edge computing devices in digital distribution networks," *IEEE Trans. Power Syst.*, vol. 39, no. 4, pp. 5712-5725, 2024.

[39] M. Salish, K. Ashwin, P. Jimmy. "Robust constrained model predictive voltage control in active distribution networks," *IEEE Trans. Sustain. Energy*, vol. 12, no. 1, pp. 400-411, 2021.

[40] Y. Huo, P. Li, H. Ji, *et al.*, "Data-driven coordinated voltage control method of distribution networks with high DG penetration," *IEEE Trans. Power Syst.*, vol. 38, no. 2, pp. 1543-1557, 2023.

Ziqi Zhang (Graduate Student Member, IEEE) received the B.S. and M.S. in electrical engineering from Tianjin University, China, in 2019 and 2022, respectively.

He is currently pursuing the Ph.D. degrees in electrical engineering in Tianjin University. His current research interests include distributed generation and optimal operation of active distribution networks.

Peng Li (Senior Member, IEEE) received the B.S. and Ph.D. degrees in electrical engineering from Tianjin University, Tianjin, China, in 2004 and 2010, respectively.

He is currently a Professor with the School of Electrical and Information Engineering, Tianjin University. His current research interests include operation and planning of active distribution networks, modeling, and transient simulation of power systems. Prof. Li is an Associate Editor of IEEE Transactions on Sustainable Energy, CSEE Journal of Power and Energy Systems, Sustainable Energy Technologies and Assessments, and IET Renewable Power Generation.

Haoran Ji (Senior Member, IEEE) received the B.S. and Ph.D. degrees in electrical engineering from Tianjin University, Tianjin, China, in 2014 and 2019, respectively.

From 2019 to 2021, he was a Postdoctoral Research with Tianjin University. He is currently an Associate Professor with Tianjin University. His research interests include distributed generation systems and optimal operation of distribution networks. He was supported by China National Postdoctoral Program for Innovative Talents.

Hao Yu (Senior Member, IEEE) received the B.S. and Ph.D. degrees in the electrical engineering from Tianjin University, Tianjin, China, in 2010 and 2015, respectively. He is currently an Associate Professor with the School of Electrical and Information Engineering, Tianjin University, Tianjin, China.

His current research interests include the operation analysis and optimization of active distribution networks and integrated energy systems. He is the assistant editor of IET Energy Systems Integration.

Jinli Zhao (Member, IEEE) received the Ph.D. degree in electrical engineering from Tianjin University, Tianjin, China, in 2007. She is currently an Associate Professor in the School of Electrical and Information Engineering, Tianjin University.

Her research interests include operation and planning of active distribution networks, and power system security and stability.

Wei Xi received the M.S. degree in electrical engineering from Huazhong University of Science and Technology, Wuhan, China, in 2003.

He is currently the Novel Electric Power System (Beijing) Research Institute of China Southern Power Grid. He is also pursuing the Ph.D. degree in electrical engineering, in Tianjin University, Tianjin, China.

His current research interests include electric power chip development and digitization of power grid.

Jianzhong Wu (Fellow, IEEE) received the B.Sc., M.Sc., and Ph.D. degrees in electrical engineering from Tianjin University, China, in 1999, 2002 and 2004, respectively. From 2004 to 2006, he was at Tianjin University, where he was an Associate Professor. From 2006 to 2008, he was a Research Fellow at the University of Manchester, Manchester, U.K. He is a Professor of Multi-Vector Energy Systems and the Head of the School of Engineering, Cardiff University, U.K. His research interests include integrated multi-energy infrastructure and smart grid. He is Co-Editor-in Chief of Applied Energy. He is the Co-Director of U.K. Energy Research Centre and EPSRC Supergen Energy Networks Hub.